Article
Vol. 25, No. 1, p. 19–31, February 2021
https://doi.org/10.1007/s12303-020-0043-6
pISSN 1226-4806 eISSN 1598-7477
Geosciences Journal GJ

Spatiotemporal patterns of the 2020 Haenam earthquake sequence, South Korea: lineament and migration implying fluid-driven earthquake swarm

Minkyung Son[1]*, Chang Soo Cho[1], Jin-Hyuck Choi[2], Jeong-Soo Jeon[1], and Yun Kyung Park[1]

[1]Earthquake Research Center, Korea Institute of Geoscience and Mineral Resources, 124 Gwahak-ro, Yuseong-gu, Daejeon 34132, Republic of Korea
[2]Center for Active Tectonics, Korea Institute of Geoscience and Mineral Resources, 124 Gwahak-ro, Yuseong-gu, Daejeon 34132, Republic of Korea

ABSTRACT: From late April 2020, 71 consecutive earthquakes with low magnitudes (the largest, M_w 3.2) were catalogued in the county of Haenam, South Korea. In this region, moderate to strong earthquakes were not reported by instrumental, historical, and geological records. We identified 155 uncatalogued events in the source region that occurred between April 25, 2020 and May 8, 2020 and determined the hypocenters of the 226 catalogued and detected events with relative meter-scale location errors based on the cross-correlation approach with data from permanent seismic networks. The clear lineament of the hypocenter distribution defines the fault plane as being 0.3 km by 0.3 km at a depth of ~20 km, trending WNW-ESE with a dip of ~70° in the SSW direction. The retrieved moment tensor of the largest event presents a strike of 98°, a dip of 65°, and a rake of 7°, which is close to the inferred fault geometry from relocation results. The hypocenters of the earthquake sequence progressed toward the upper east along the fault-strike direction until the largest event occurred on May 3, 2020 with left-lateral strike-slip motion at the shallower part of the fault plane where the migration is headed. We discuss potential mechanisms that cause non-volcanic earthquake swarms and suggest that the spreading of fluid flow induced the migratory behavior of the Haenam earthquake sequence. This conception of a fluid-driven earthquake swarm is supported by the presence of a seismic migration front that is comparable to a hydraulic diffusivity of 0.012 m^2/s in conjunction with inherited WNW-ESE structural sets showing a fault-fracture mesh geometry that can channel the fluid flow. The final part of the sequence forming boundary of the hypocenter distribution could be interpreted as the possible fault-valve behavior at the western end and the permeability barrier at the eastern end, respectively. Our spatiotemporal patterns of the 2020 Haenam earthquake sequence are valuable for understanding earthquake swarms in intraplate stress fields.

Key words: the 2020 Haenam earthquake sequence, hypocenter relocation, template matching, earthquake swarm, fluid diffusion

Manuscript received August 19, 2020; Manuscript accepted September 23, 2020

1. INTRODUCTION

Several small earthquakes were observed within a period of one month from the end of April 2020 in the county of Haenam, located in the southwestern part of the Korean Peninsula, South Korea. The largest event with a magnitude of 3.1 occurred on May 3, 2020 (Korea Meteorological Administration; KMA, 2020). The seismic event catalogue of Korea Institute of Geoscience and Mineral Resources (KIGAM) reports 71 events that occurred around the epicenter of the largest event (34.6–34.7°N, 126.35–126.4°E) from April 26, 2020, to May 8, 2020 (red filled circles in Fig. 1; see Table S1 in the electronic supplementary material for the event catalogue). In this study, we refer to these consecutive earthquakes as the 2020 Haenam earthquake sequence. No damages and casualties were reported because of the earthquakes; however, the local inhabitants felt the largest earthquake (KMA, 2020).

The 2020 Haenam earthquake sequence is characterized by a cluster of seismic events with a similar magnitude. The largest event occurred after about one week of the beginning of the

*Corresponding author:
Minkyung Son
Earthquake Research Center, Korea Institute of Geoscience and Mineral Resources, 124 Gwahak-ro, Yuseong-gu, Daejeon 34132, Republic of Korea
Tel: +82-42-868-3971, Fax: +82-42-861-1872, E-mail: kersti@kigam.re.kr

Electronic supplementary material
The online version of this article (https://doi.org/10.1007/s12303-020-0043-6) contains supplementary material, which is available to authorized users.

sequence, which differs from commonly occurring seismic behaviors typically characterized by a foreshock-mainshock-aftershock sequence (e.g., Mogi, 1963). This observation might provide significant implications for the existence of an earthquake swarm on the southwestern Korean Peninsula, a tectonically stable intraplate region.

We begin by searching for seismicity in instrumental, historical, and geological records around the source region of the 2020 Haenam earthquake sequence. We then identify uncatalogued earthquakes based on waveform similarity and relocate hypocenters of the sequence by using data from the networks of permanent seismic stations based on a hierarchical clustering of waveforms. We describe the spatiotemporal characteristics of the hypocenter distribution on the inherited geological structures and the migratory behavior of the earthquakes. We investigate potential sources for the sequence including the fluid-diffusion process, which can provide valuable information on the developing mechanisms of intraplate earthquake swarms.

2. SEISMICITY AND TECTONIC SETTING

Neotectonic deformation in the Korean Peninsula located on the Eurasian plate results mostly from the subduction of the Pacific plate and the Indian-Eurasian collision. Seismotectonic studies were mainly conducted in the southeastern part of the Korean Peninsula due to geological evidence of surface-faulting paleo-earthquakes along the major structures and recent moderately sized damaging earthquakes (e.g., 2016 M_w 5.5 Gyeongju earthquake and 2017 M_w 5.4 Pohang earthquake). The results show that tectonic stress is primarily accommodated by pre-existing structures inherited in major fault systems (Choi et al., 2019) and the principal compressive stress has a direction of 070–090° (Soh et al., 2018).

Seismotectonics has rarely been studied in the southwestern part of the Korean Peninsula due to the absence of reports on the occurrence of moderate to strong earthquakes in both instrumental and geological records. Recent minor earthquakes have been used to a limited extent in investigating the seismicity and neotectonics of this region. Jung and Kyung (2013) argue that the direction of the nodal planes of the 22 small earthquakes (M_L 2.0–3.5) that occurred from January 2005 to March 2011 in the region (34–36°N, 126–128°E), are almost parallel to the general trends of lineaments, 'NNE-SSW and WNW-ESE' or 'NE-SW and NW-SE.'

The 2020 Haenam earthquake sequence occurs at the southwestern part of the NE-SW trending Okcheon Belt that belongs to one of the major tectonic domains in the Korean Peninsula. This region is composed of Paleoproterozoic to Jurassic granites and Cretaceous sedimentary and volcanic rocks (Kee et al., 2020). Two structural sets are inherited in these basement rocks (Fig. 1): (1) a NNE-SSW trending major strike-slip fault, the Gwangju Fault, and its subsidiary sub-vertical faults; and (2) WNW-ESE trending and high-angle dipping faults widely distributed over the region. The latter set has no major fault and hence, it is discontinuously traced on the map. The WNW-ESE trending faults and fracture zones are passages of district-scale hydrothermal fluid flow through the Upper Mesozoic strata, and thus the location of ore bodies is strongly controlled by this structural set (Koh and Chang, 1997; Yang et al., 2013; Ryoo et al., 2014).

The KIGAM seismic event catalogue (last accessed: May 11, 2020) reports that 121 events occurred in the area (34.5–34.8°N, 126.2–126.6°E) within a radius of ~20 km from the epicenter of the largest of the 2020 Haenam earthquake sequence (red open and filled circles in Fig. 1).The seismic event catalogue of the KIGAM has been archived digitally since September, 1997. The earliest of the 121 events occurred in November 2003. Note that the first few years of the KIGAM catalogue does not have homogeneity in event reporting, although the performances of seismic networks used in the catalogue have improved through the installation of new seismic stations (e.g., Sheen and Shin, 2010; Shin et al., 2019).

The historical (AD 2–1904) earthquake catalogue for the Korean Peninsula, produced as part of the seismic hazard map revision task by the National Emergency Management Agency (NEMA, 2012; Choi et al., 2014), reported seven earthquakes in the area within 34.45–34.85°N, 125.95–126.75 (green circles in Fig. 1). According to the historical earthquake catalogue, these seven earthquakes occurred during the period of the Joseon Dynasty and their magnitudes were inferred to have been 3.2–4.0. The largest of the seven historical earthquakes occurred in April 1549, ~45 km away from the source region of the 2020 Haenam earthquake sequence. The January 1686 event is the latest of the seven historical earthquakes, and it is also the nearest (~10 km) to the source region of the 2020 Haenam sequence.

3. DATA AND METHODS

3.1. Waveform Classification and Detection Based on Cross-correlation Approach

We performed waveform classification for the catalogued events that occurred within the study area to inspect the seismicity related to the 2020 Haenam earthquake sequence. The waveforms from stations MUN and AJD were analyzed as these are the oldest stations in the study area. Furthermore, the sensors and recorders installed at MUN and AJD have not been changed since 2013. Of the 121 earthquakes that have been catalogued from 1997 by KIGAM (last accessed: May 11, 2020; see open and closed red circles in Fig. 1), 106 and 100 events were recorded

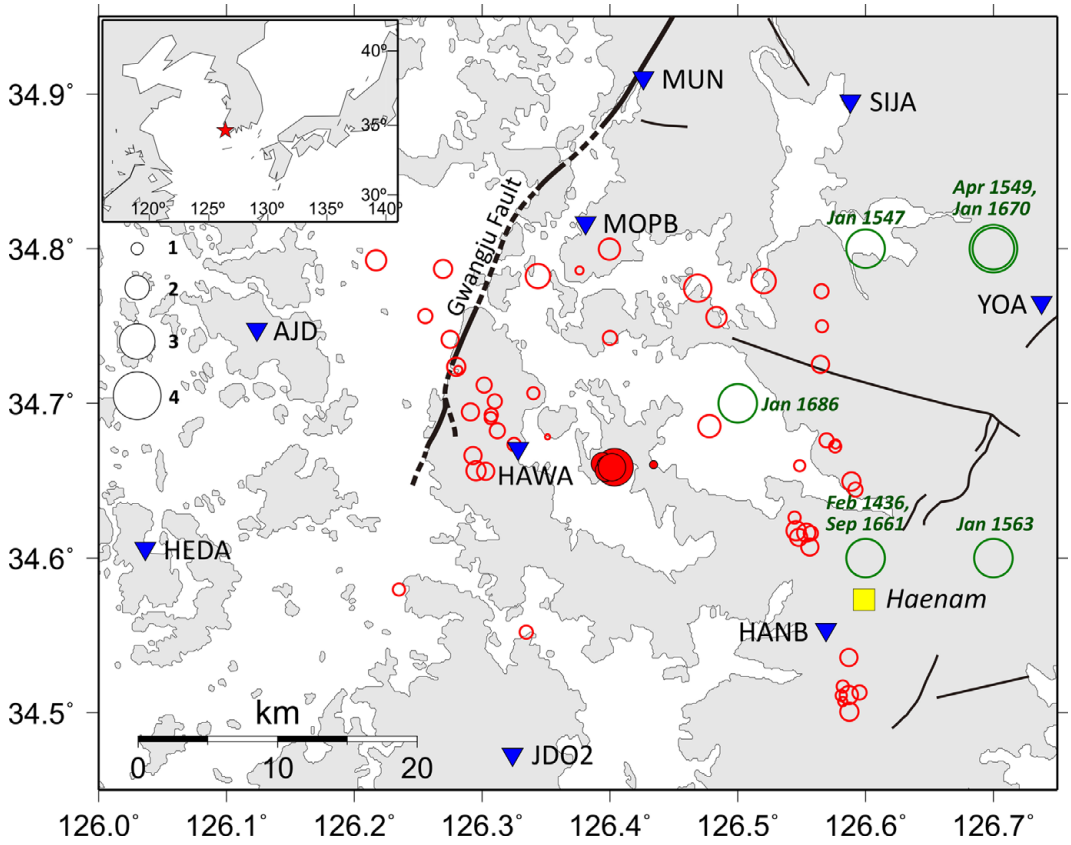

Fig. 1. Map of the 2020 Haenam earthquake sequence. Red filled circles represent the 71 catalogued events of the sequence. Red open circles represent the 50 events catalogued in the region around Haenam, South Korea (34.5–34.8°N, 126.2–126.6°E) from September 1997. Green circles are for the historical earthquakes of seven that occurred on the southwestern part of the Korean Peninsula during the Joseon Dynasty period. The geological fault traces were obtained from the study conducted by Kee et al. (2020).

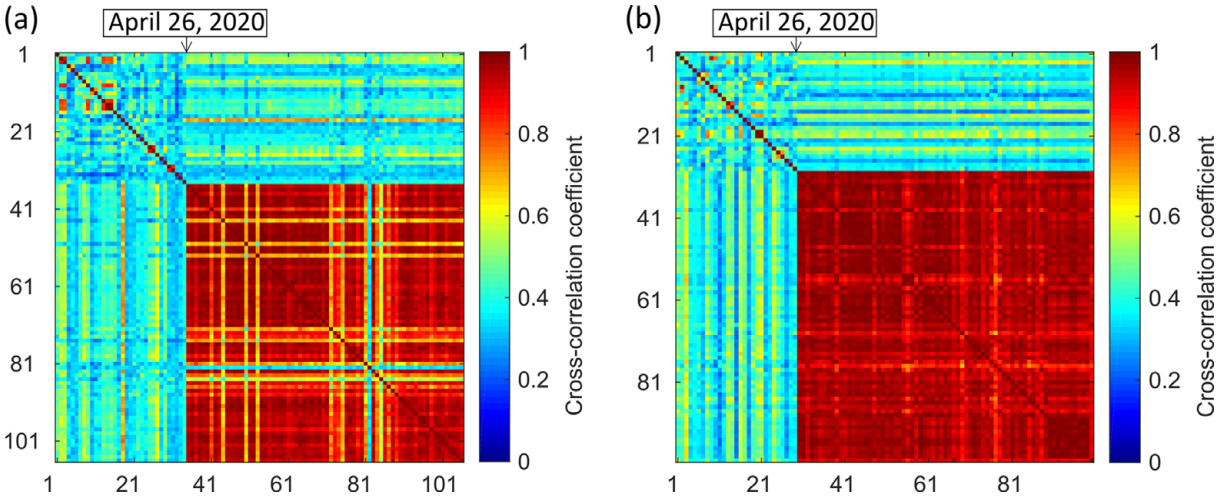

Fig. 2. The maximum cross-correlation coefficient matrix for waveforms of the events within an area of ~20 km radius from the epicenter of the largest event of the 2020 Haenam earthquake sequence. The waveforms recorded at station (a) MUN and (b) AJD were employed in the cross-correlation with band-pass filtering between 2 Hz and 8 Hz.

by stations MUN and AJD, respectively. We computed the cross-correlation coefficients (CC) matrix for these events with a time-window covering the peak amplitude to define waveform similarities between each other. The correlation coefficient matrix displays a significantly high value among the events that occurred after April 26, 2020 when the KIGAM event catalogue began reporting the 2020 Haenam earthquake sequence (Fig. 2).

In addition, we searched for uncatalogued events by waveform

https://doi.org/10.1007/s12303-020-0043-6

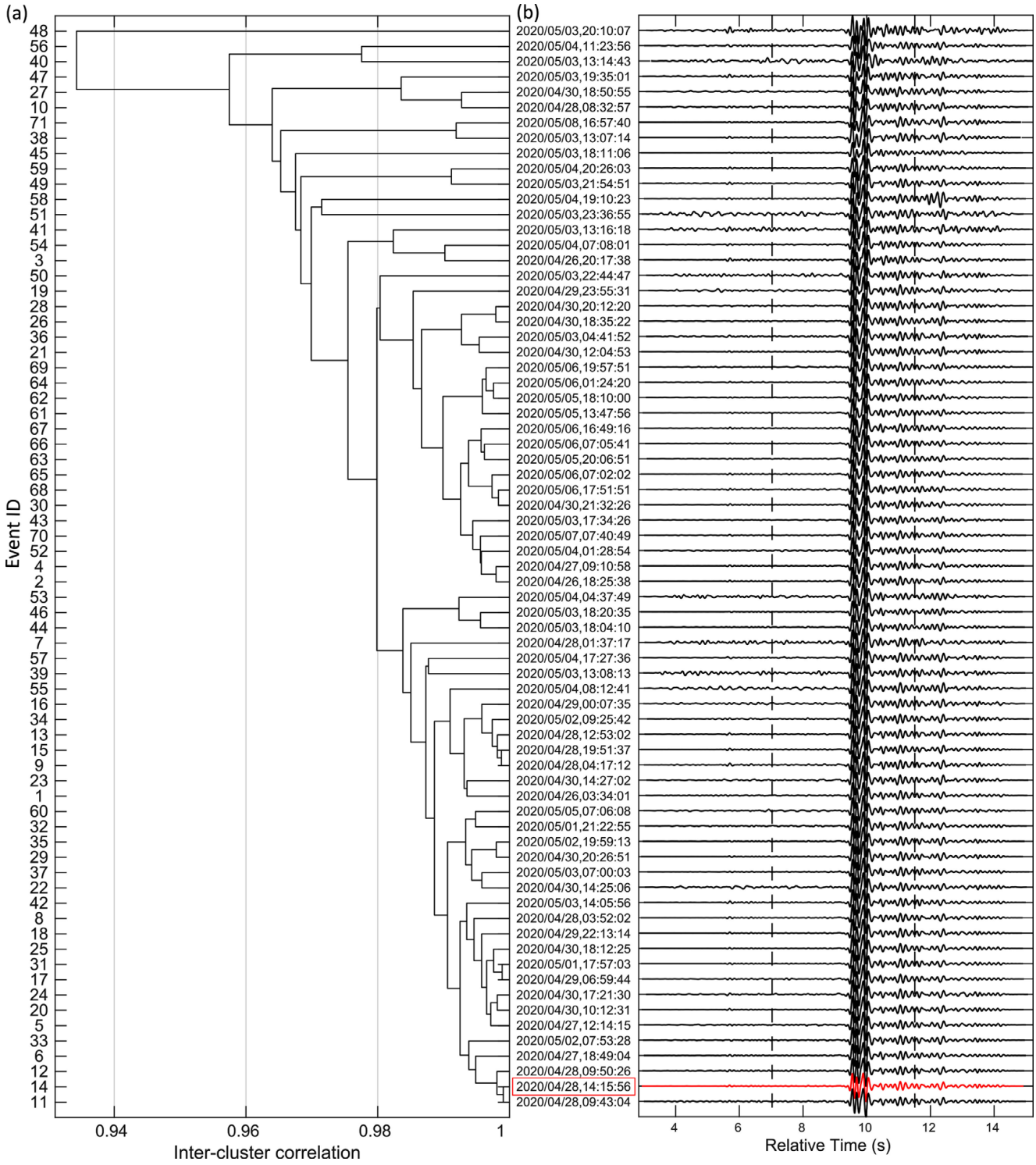

Fig. 3. Hierarchical clustering of the waveforms of the 71 catalogued events in the 2020 Haenam earthquake sequence: (a) dendrogram (hierarchical cluster tree); (b) classified waveforms according to the dendrogram. The template waveform for the uncatalogued event detection is colored in red (b), which is the largest magnitude event among the most linked event pair, the two events at the bottom of the dendrogram with the shortest branch height. The dashed lines in (b) are for the time-window used in the template matching technique for the uncatalogued event detection.

cross-correlation between a template trace and the seismic waveform continuously recorded by station AJD from March 7, 2013 to May 11, 2020. As a template, we used the waveform of the event with the shortest branch of the dendrogram for the waveforms of the 71 catalogued events (i.e., the most linked event in Fig. 3a; April 28, 14:15:56 UTC). The dendrogram presents similar

waveform events close together with branch heights corresponding to one minus the averaged CC (Fig. 3a). Thus, we considered the event with the shortest branch to be representative of the 71 catalogued event waveforms (red trace in Fig. 3b).

The CC matrix used in the dendrogram construction was computed for the waveforms of the N-S velocity component of station AJD. The N-S component waveform was empirically selected because of its large-amplitude surface waves, which might increase the signal-to-noise ratio. The band-pass filter from 2 to 8 Hz was applied to the waveforms of the 71 catalogued events, which is the same as the bandwidth of the template trace and continuous waveform. The time-window for the template trace that began from 7 s after its origin time continued for 4.5 s to cover S- and surface-waves (dashed lines in Fig. 3b). The detection criterion was set to the maximum cross-correlation coefficients larger than 0.7 after visual inspection of the time series of the maximum CC. The local magnitudes of the detected events were determined by the relationship provided in Shin et al. (2005).

3.2. Hypocenter Relocations and Fault Solution Determination

We relocated hypocenters of the 2020 Haenam earthquake sequence including the catalogued and detected events by using GrowClust (Trugman and Shearer, 2017), a relative earthquake relocation algorithm based on hierarchical clustering of waveform similarity. The location uncertainty was estimated by GrowClust's bootstrap approach with resampled travel-time difference data.

The relocation used the 73,174 of travel-time differences for P- and S-waves and the cross-correlation coefficients corresponding to the pairs for travel-time differences. The correlation coefficients were employed in grouping events into clusters. The utilized waveforms are from the permanent stations, AJD, MUN, HEDA, HANB, HAWA, JDO2, MOPB, SIJA, and YOA in the seismic networks operated by KIGAM and KMA. During data processing, the records were chosen by the following priority ordering of sensors: short-period, broadband seismometers, and then accelerometers.

For the relocation, we assigned initial locations to the newly detected events that were unrecorded in the catalogued information. The initial locations were from random perturbation with the averaged hypocenter of the catalogued events. This random assignment of initial locations to the uncatalogued events was successfully applied to the relocation of the 2013 Baekryeong earthquake sequence on the Korean Peninsula (Son et al., 2015).

The moment tensor solution for the largest event of the 2020 Haenam earthquake sequence was determined by a time-domain waveform inversion method (Dreger, 2003; Minson and Dreger, 2008). Time-shifting based on waveform cross-correlation (Son et al., 2018) could accommodate possible uncertainties of the velocity model of Kim et al. (2011). The inversion used waveform data with a frequency of 0.45–0.85 Hz from permanent broadband stations (BGDB, BGD, YGN, and JEO2).

4. RESULTS

4.1. Detected Events and their General Trends

We identified 155 hitherto unidentified events in the 2020 Haenam earthquake sequence after cross-correlating the continuous waveform of station AJD with template records. Figure 4a shows the cross-correlation coefficients between the template record and the continuous waveform recorded from March 2013 to early May 2020 at station AJD. The cross-correlation coefficients for ~7 years are usually smaller than 0.7 (Fig. 4a), and 161 temporal points had coefficients larger than 0.7. It is notable that the cross-correlation for the period in 2020 (pink-shaded period in Fig. 4a) produces coefficients higher than 0.7 in addition to the coefficients lower than 0.7. The event sequence with the cross-correlation coefficients higher than 0.7 appear from April 25, and disappear on May 8, 2020 (Fig. 4b), which indicate that the 2020 Haenam earthquake sequence began on April 25, 2020, one day before the first catalogued event occurrence. A pattern of day-night cycle is visible in Figure 4b, which implies the validity of the seismic event detection based on cross-correlation coefficients. The clear alignment of the waveforms (Fig. 4c) not only ensures the reliability of the detection based on waveform similarity but also suggests the hypocenter proximity of the 226 events.

The seismicity of the 2020 Haenam earthquake sequence has an increasing trend until April 30, 2020 (Fig. 5a) and becomes relatively low during the next two days (May 1–2; Fig. 5a). The seismicity becomes active again with the largest event of the sequence on May 3, 2020 (Fig. 5a). The local magnitudes of the 155 detected and the 71 catalogued events range from 0.4 to 3.2 (circles in Fig. 5a).

The seismic b-value, an absolute value of the gradient of solid line in Figure 5b, is estimated as 0.92 with the completeness magnitude of 0.5. Seismic b-values around 0.6–1.0 are typical for mainshock-aftershock sequences in tectonic environments (e.g., Kagan, 1997; Schorlemmer et al., 2005). The b-value 0.92 for the 2020 Haenam earthquake sequence is slightly lower than the b-value 0.98 for the 2016 Gyoengju earthquake sequence on the southeastern Korean Peninsula, estimated by Woo et al. (2019).

There are temporal changes in the b-value for the 2020 Haenam earthquake sequence, which ranges from ~0.9 to ~1.3 (Fig. 5c). It is noteworthy that the b-values for the period around the occurrence of the largest event are comparable to the b-value of

https://doi.org/10.1007/s12303-020-0043-6

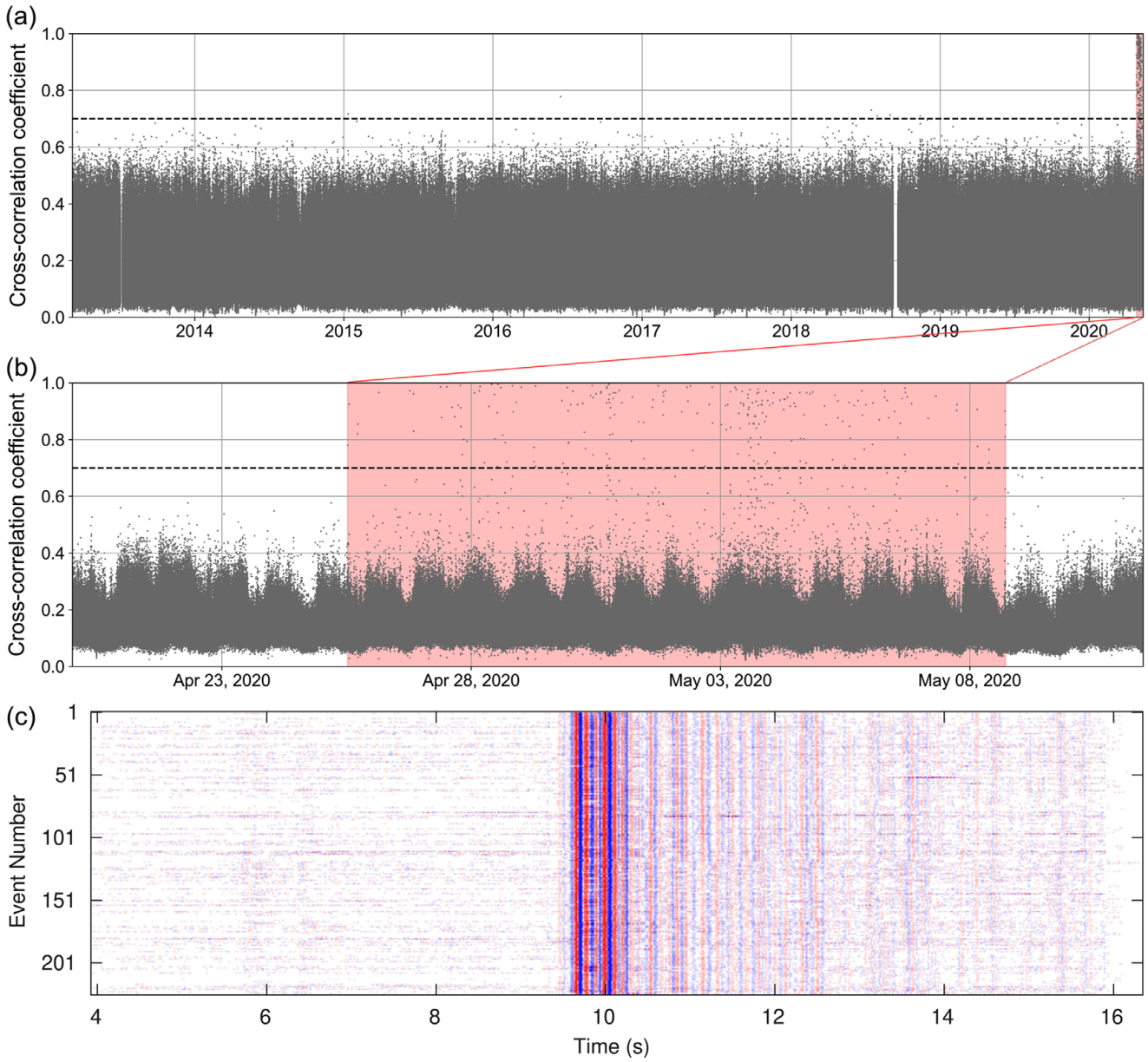

Fig. 4. Detection of the uncatalogued seismic events for the 2020 Haenam earthquake sequence based on the template matching method with waveform cross-correlation: time series of the maximum cross-correlation coefficients representing waveform similarity for (a) the period from March 7, 2013 to May 11, 2020; (b) same as (a) but zoomed in, for the 2020 Haenam sequence; (c) waveforms of the 71 catalogued and 155 detected events, recorded at station AJD for the N-S component with band-pass filtering from 2 Hz to 8 Hz. The temporal gap in (a) represents the period of 12 days in September 2018 when the continuous data of station AJD were not archived. The pink-shaded period and dashed line in (a) and (b) denoted the period of the 2020 Haenam sequence and CC larger than 0.7, respectively. Each trace in (c) was normalized and shaded with blue = –1 and red = 1 amplitude, and events in (c) are ordered from earliest to latest, and the event number increases with the origin time.

~1.2 estimated for the swarm-type earthquakes in the Long Valley Caldera and the adjacent Sierra Nevada (e.g., Hill et al., 2003). High b-values (> 1) can indicate an earthquake sequence enriched in small earthquakes. However, a couple of days of high b-values alone is not sufficient diagnostic criteria for an earthquake swarm, because an increase in b-value can be observed after a mainshock (Gulia et al., 2018).

4.2. Clear Lineament of Hypocenter Distribution

Three of the initial location distributions were examined for the 155 newly detected events that were absent from the catalogued location (see the top row of Fig. 6) for the hypocenter relocation. The relocated hypocenters of the 71 catalogued and 155 newly detected events extend ~300 m along the WNW-ESE direction

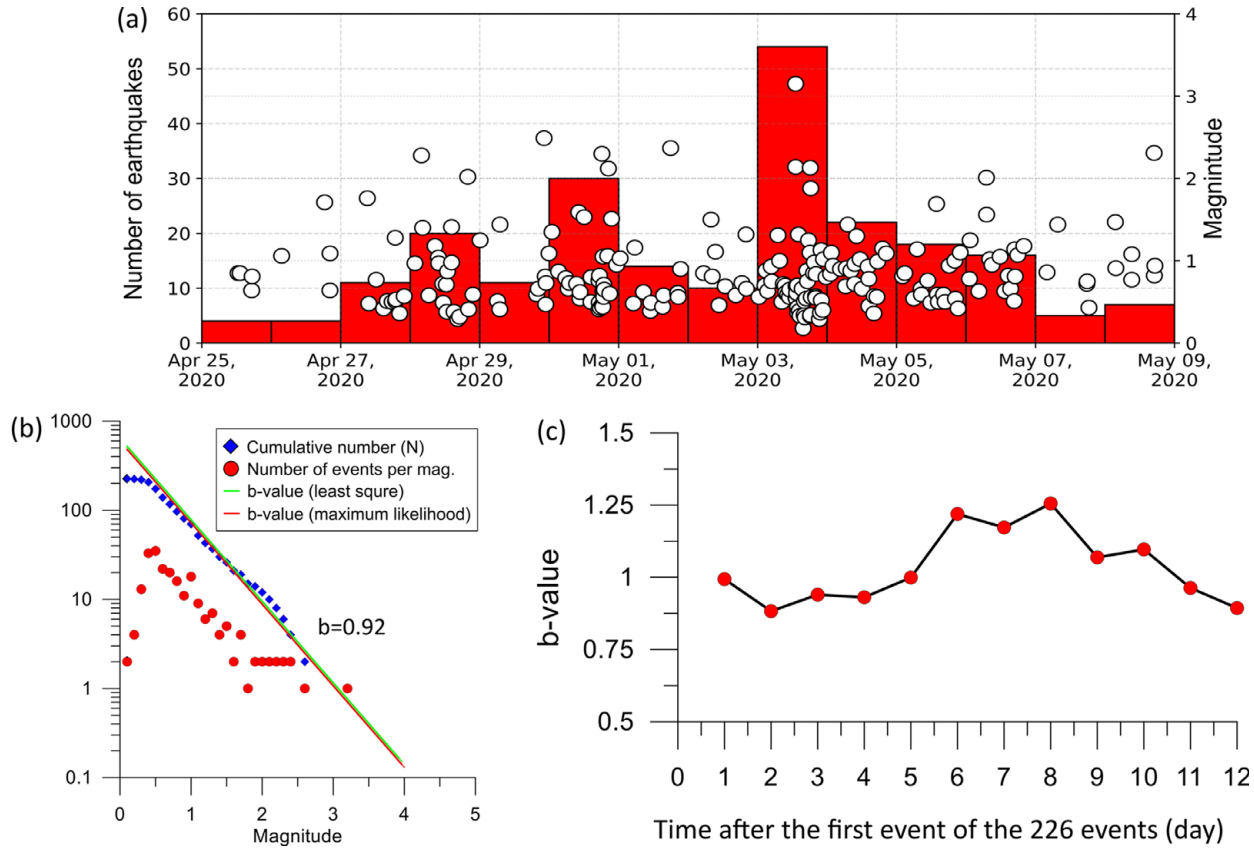

Fig. 5. Statistics of the 2020 Haenam earthquake sequence: (a) chronology of the earthquake sequence during the period April 25, 2020 to May 8, 2020; (b) frequency-magnitude distribution through the whole period of interest; and (c) temporal changes in Gutenberg-Richter b-value during the period of interest.

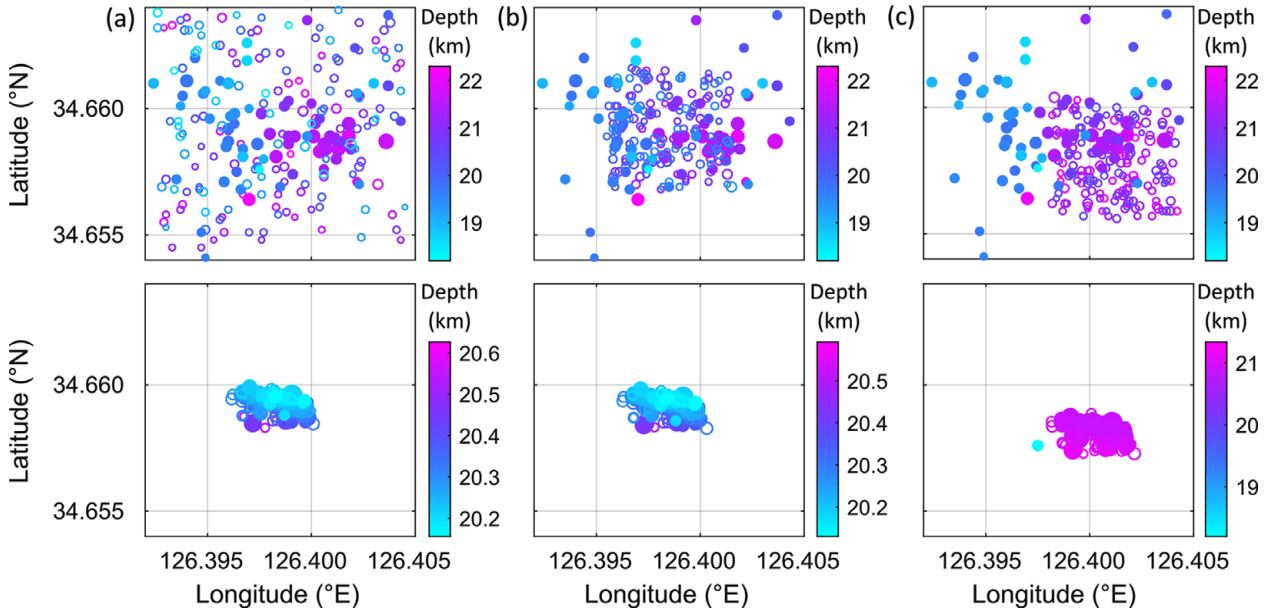

Fig. 6. Hypocenter relocation for 226 events in the 2020 Haenam earthquake sequence: the top and bottom rows are for the initial and relocated hypocenters, respectively. The initial location for the 155 detected events was assigned from the random perturbation, (a) with the averaged hypocenters of the 71 catalogued events for a whole hypocentral area of the catalogued events, (b) with the averaged hypocenters for the 71 catalogued events for a quarter of the catalogued hypocentral area, and (c) with the location of the template events used in the event detection for a quarter of the catalogued hypocentral area. The closed and open circles are for the catalogued and detected events, respectively. The color scale represents depth range; but note that the depth range is different for each map.

https://doi.org/10.1007/s12303-020-0043-6

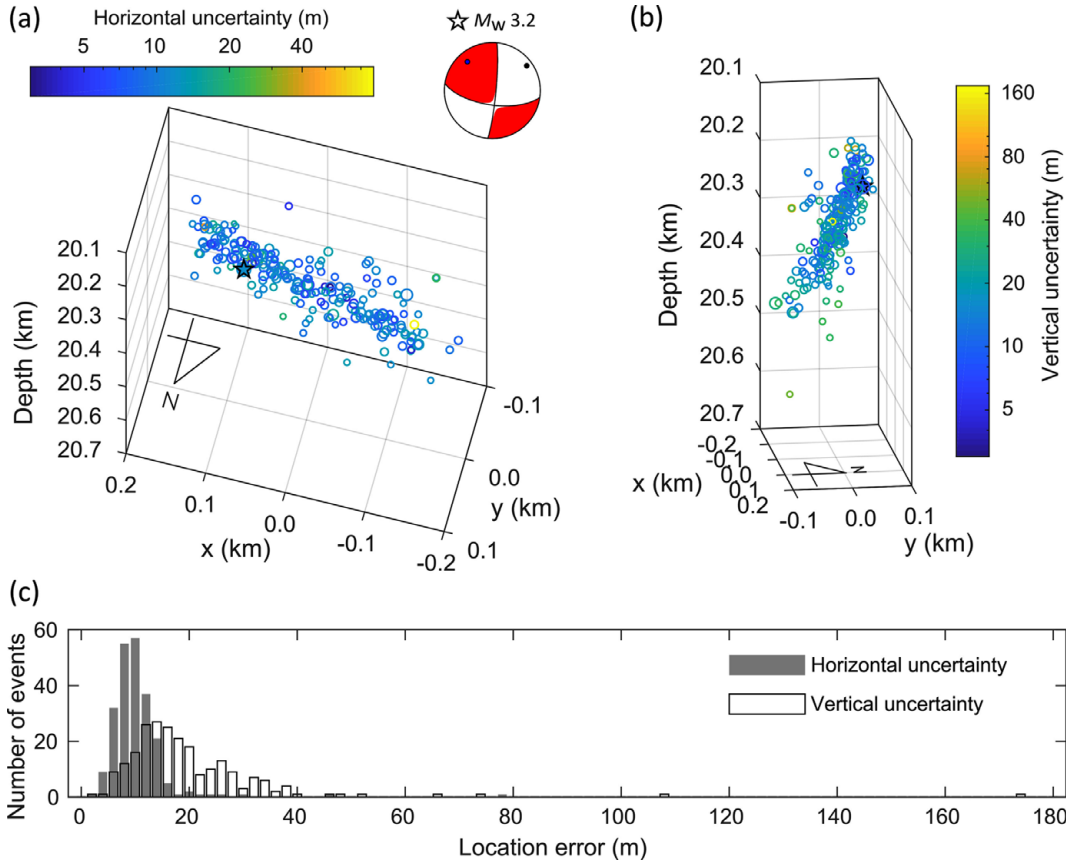

Fig. 7. The 226 relocated hypocenters of the 2020 Haenam earthquake sequence in (a) dip view and (b) strike view, with (c) the location uncertainty. The color scale represents location error ranges; but note that the error range is different in (a) horizontal and (b) vertical. The star represents the hypocenter of the largest event (M_w 3.2).

and deepening SSW (see the bottom row of Fig. 6). The depth range of the relocated hypocenters differs according to the initial locations; however, the relative depth distribution remains stationary (Fig. 6). We chose the hypocenter relocation result in Figure 6a, to avoid bias in terms of depth range.

The 226 relocated hypocenters of the catalogued and newly detected events form linear patterns in dip and strike views (Figs. 7a and b), which suggests a single fault plane at a depth of 20.2 km to 20.5 km (Figs. 7a and b). The moment tensor of the largest event (M_w 3.2) presents left-lateral strike-slip faulting with a strike of 98° and a dip of 65°, which correspond to the defined lineaments of the hypocenter distribution (see the beach-ball diagram in Fig. 7a; detailed information on the moment tensor solution is provided in the electronic supplementary material).

The events deviating from the lineament have high relocation uncertainties (see circles on the light green to yellow scale in Figs. 7a and b), which support the reliability of our identification of the fault plane based on the spatial distribution of the relocated hypocenters. The median values in the horizontal errors of the relative locations is 10 m, which is approximately half that of the vertical errors of 17 m (Fig. 7c). The standard deviations of the horizontal and vertical errors are 6.3 m and 15.4 m, respectively.

4.3. Spatiotemporal Characteristics of Hypocenter Distribution

We defined the evolution of the 2020 Haenam earthquake sequence based on the 226 relocated hypocenters of the sequence. The events of the early part in the sequence (blue circles in Figs. 8a and b) occur at the southwestern part of the inferred fault plane. The sequence progressed northeast wards (Fig. 8a), which corresponds to upward migration in the depth direction (Fig. 8b). The largest event (M_w 3.2) occurs at the shallower part of the fault plane where the sequence is headed (Fig. 8b). Soon after the occurrence of the largest event, the sequence produces events on not only the whole part of the fault plane but also at both ends of the fault plane (yellow circles in Fig. 8c). It is interesting that the final part of the sequence develops in the western side of the fault plane extending ~0.1 km into the west (red circles in Fig. 8c), whereas the events of the final part are confined to the eastern side of the fault plane (deep red in Fig. 8c).

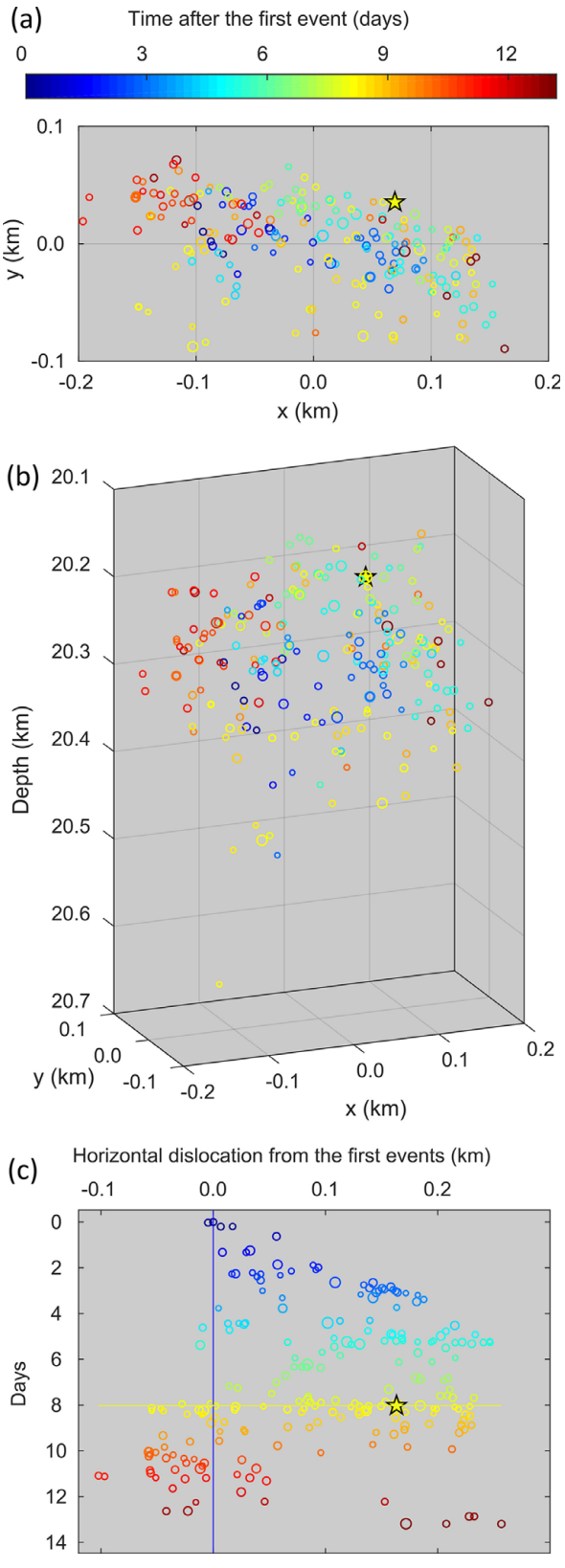

Fig. 8. Spatiotemporal distribution of the relocated hypocenters for the 2020 Haenam earthquake sequence in (a) map view, (b) view for the inferred fault plane, and (c) horizontal direction. The circles are for the 226 events and the star represents the largest event with a magnitude of M_w 3.2.

5. DISCUSSION

5.1. Nature of Earthquake Swarm

Earthquakes sequences are attributed to long-term seismic cycles that occur mostly on major inter-plate faults, aftershocks triggered by large earthquakes, and earthquake swarms. As there was no remarkable mainshock event associated with the 2020 Haenam earthquake sequence in a tectonically stable intraplate region, we discuss mechanisms associated with the presence of an earthquake swarm. Earthquake swarms are commonly associated with magmatic events, in particular, before and during volcanic eruptions: Redoubt Volcano, Alaska (e.g., Chouet et al., 1994); Axial Volcano, Juan de Fuca Ridge (Dziak and Fox, 1999); and Miyakejima Volcano, Japan (e.g., Geshi et al., 2002). Here, we do not consider a volcanic event as a source of the 2020 Haenam earthquake sequence because there is no volcanic activity in the region. Therefore, we consider possible mechanisms for the earthquakes as those associated with spreading fluid or hydrothermal circulation (e.g., Yellowstone Lake; Mammoth Mountain, California) (Farrell et al., 2010; Shelly et al., 2015) and fault creep (i.e., aseismic slip) (e.g., Lohman and McGure, 2007; Shelly et al., 2011).

We argue that it is difficult to infer possible aseismic slips of the WNW-ESE trending faults for the following reasons. In this inherited fault set, there is no major fault that accommodates tectonic stress. This argument is supported by the fact that no reports on geodetic deformation and surface faulting associated with large earthquakes are available for the region. Furthermore, migration velocity of about 0.04 km/day for the 2020 Haenam earthquake sequence is much slower than well-documented creep events although they vary depending on deformation rates of regions (e.g., Lohman and McGuire, 2007).

We focus on the roles of pre-existing structures interacting with fluid below the source region. The inferred movement of the largest event in the 2020 Haenam earthquake sequence can be explained by a WNW-ESE trending fault inherited in the basement rocks that are rupturing with a sinistral motion. In the field, we observe that the WNW-ESE trending fault set on the source area is characterized by a widely distributed geometry without a major fault, instead, intensive fractures and/or veins around each fault are seen (Koh and Chang, 1997; Yang et al., 2013; Ryoo et al., 2014). This structural pattern implies that the WNW-ESE trending fault set has a fault-fracture mesh geometry. The inferred fault mesh corresponds to the results of previous studies that present the relationship between fluid diffusion and migrating earthquake swarms (Shelly et al., 2015; Ruhl et al., 2016).

https://doi.org/10.1007/s12303-020-0043-6

5.2. Earthquake Migration Driven by Fluid Flow on Fault-Fracture Mesh

The migratory behavior of earthquakes has been reported for the foreshock sequence (e.g., Chen et al., 2011; Kato et al., 2016), aftershock sequence (e.g., Peng and Zhao, 2009; Ross et al., 2017), and swarm-type earthquakes (e.g., Shelly et al., 2015; Ruhl et al., 2016). We focus on the fact that migrating earthquakes are commonly analyzed by comparing migration distance and occurrence time to hypothetical curves based on a diffusion model from a point source (e.g., Shapiro et al., 1997; Shelly et al., 2015). We used the relationship,

$$r = \sqrt{4\pi \times D \times t}\,, \quad (1)$$

where is the distance, is the hydraulic diffusivity, and the is the time (Shapiro et al., 1997). The diffusion curve with 0.012 m^2/s matches the seismic migration front of the 2020 Haenam earthquake sequence (Fig. 9). The value for the diffusivity lies within the range of typical values for the crust (0.01–10 m^2/s; Talwani and Acree, 1984; Scholz, 2002; Parotidis et al., 2005; Hatch et al., 2020), though a well-documented value for the hydraulic diffusivity across the source area is unavailable.

The depth of the hypocenters associated with the 2020 Haenam earthquake sequence is about 20 km, which corresponds to the base of the seismogenic depth in the Korean Peninsula. We note that the 2013 Boryeong earthquake swarm also occurred at a depth of about 20 km (Son, 2016). Thus, the 2020 Haenam earthquake sequence could be associated with intrusions of fluid into the seismogenic depth throughout the fault-fracture mesh. This interpretation with regard to the fluid-faulting interaction on the fault-fracture mesh structure can be supported by the inherited structures trending WNW-ESE with the ore bodies of hydrothermal origin, though the mineralization induced by hydrothermal fluid was inferred as a pre-neotectonic event (Upper Mesozoic; Koh and Chang, 1997; Yang et al., 2013; Ryoo et al., 2014).

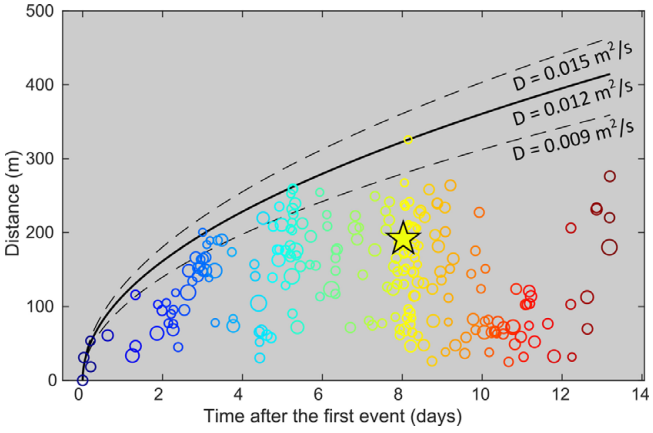

Fig. 9. Seismicity front of the 2020 Haenam earthquake sequence, following a diffusion process with a diffusivity of 0.012 m^2/s. The open circles are for the 226 events of the 2020 Haenam earthquake sequence, and their color scale is for temporal order as shown in Figure 8. The star represents the largest event (M_w 3.2) of the sequence. The dashed and solid lines are for curves with the noted diffusion rates.

We infer that the fluid is naturally injected into the hypocenter of the first event in the sequence (see Figs. 8c and 9) as suggested by previous studies on migrating earthquake swarms (e.g., Ruhl et al., 2016; Ross et al., 2020). The spreading fluid on the fault plane triggers consecutive events and guides the migration of seismicity moving their hypocenters eastward. The largest event rupturing the whole part of the fault plane acts as a fault-valve and induces aftershocks on the fault plane (see yellow circles in the western end in Fig. 8c) and new faulting at the western end of the fault plane (see red circles in Figs. 8c and 9). The lack of migration toward the upper eastern end indicates a permeability barrier in view of fluid-rock interaction (e.g., Ross et al., 2020) (see deep red circles in Figs. 8c and 9).

5.3. Implications for Geological Structure and Fluid-Faulting Interaction

The relations between faults and earthquakes are well known, but in non-earthquake prone regions including the Korean Peninsula it is not easy to identify seismic faults for specific earthquakes. This is due to a weak correlation of spatial distribution between traces of inherited faults in the surface and foci of instrumental earthquakes. Note that here strong earthquakes involving surface ruptures during the modern history of the Korean Peninsula were not recorded. So far, investigations on the relationship between inherited faults and seismicity are limited (Han et al., 2019). Our study shows that the earthquake migration is strongly controlled by the inherited structures, which highlights the importance of studying small earthquakes to understand the roles of inherited structures on seismic behavior in intraplate regions.

Furthermore, the hypocenter migration in the 2020 Haenam earthquake sequence is the first observation of the seismic front matching fluid diffusion process on the Korean Peninsula. Recent studies have validated that migrating over-pressured fluids induced swarms of earthquakes (e.g., Cox, 2016; Ruhl et al., 2017). Sibson (2020) has emphasized the role of pore-fluid pressure driven by prograde metamorphism at depth for the lower seismogenic zone. Further studies such as critical fluid pressure analysis are required to understand (1) the hypocenter migration observed before the occurrence of the largest event; and (2) the different failure patterns on both ends of the fault plane observed after the occurrence of the largest event. These efforts provide further insights on the possible mechanisms that cause the migration of intraplate earthquakes.

6. CONCLUSIONS

We found migratory behavior in the 2020 Haenam earthquake sequence as presented by the associated fault plane extending ~0.3 km in the WNW-ESE direction with a dip of ~70° in the SSW direction. Beginning with the first event of the sequence on April 25, 2020, the hypocenters progressed toward the upper east, until the largest event (M_w 3.2) occurred where the migrating hypocenters are headed. The migration front of the seismicity is comparable to the spreading of the fluid flow with a diffusivity of 0.012 m^2/s. In view of this fluid-driven earthquake swarm, the final parts of the sequence on both ends of the fault plane could be explained by the possible second intrusion at the west edge and the possible permeability barrier at the eastern end, respectively.

The cross-correlation approach incorporating data from permanent seismic networks was successfully applied to waveform detection for uncatalogued event identification, and relative relocation of hypocenters with meter-scale location errors. The inherited structures sub-parallel to the lineament of relocated hypocenters with the ore bodies of hydrothermal origin, which indicates the possible pre-existing fault-fracture mesh channeling fluid flow in the source region. Our well-constrained hypocenter locations could be essential information for future studies, and our interpretation of the hypocenter migration might provide insights into understanding non-volcanic earthquake swarms in intraplate stress fields.

ACKNOWLEDGMENTS

We would like to thank Yun Jeong Seong for illustrating Figures 4a, b, 5a, and the analysts of the Earthquake Research Center of KIGAM for their efforts in cataloguing seismic events, especially in the case of the 2020 Haenam earthquake sequence. We also appreciate the anonymous reviewers and the Guest Editor, Kwang-Hee Kim, for their careful reading and helpful comments. Continuous waveforms were acquired from permanent seismic networks and data centers in the region including those of KIGAM and KMA (http://necis.kma.go.kr/). The geotectonic lines can be viewed at https://mgeo.kigam.re.kr/. The figures in this article were generated using Generic Mapping Tools (Wessel et al., 2013), MATLAB (https://www.mathworks.com/products/matlab.html), and InkScape, a free open-source graphic editor (https://inkscape.org/). This study was supported by the Basic Research Project of KIGAM funded by the Ministry of Science and ICT (MSIT, Republic of Korea).

REFERENCES

Chen, X., Shearer, P.M., and Abercrombie, R.E., 2012, Spatial migration of earthquakes within seismic clusters in Southern California: evidence for fluid diffusion. Journal of Geophysical Research, 117, B04301.

Choi, S.-J., Jeon, J.S., Choi, J.-H., Kim, B., Ryoo, C.-R., Hong, D.-G., and Chwae, U., 2014, Estimation of possible maximum earthquake magnitude of Quaternary faults in the southern Korean Peninsula. Quaternary International, 344, 53–63.

Choi, J.-H., Ko, K., Gihm, Y.S., Cho, C.S., Lee, H., Song, S.G., Bang, E.-S., Lee, H.-J., Bae, H.-K., Kim, S.W., Choi, S.-J., Lee, S.S., and Lee, S.R., 2019, Surface deformations and rupture processes associated with the 2017 Mw 5.4 Pohang, Korea, earthquake. Bulletin of the Seismological Society of America, 109, 756–769.

Chouet, B.A., Page, R.A., Stephens, C.D., Lahr, J.C., and Power, J.A., 1994, Precursory swarms of long-period events at Redoubt Volcano (1989–1990), Alaska: their origin and use as a forecasting tool. Journal of Volcanology and Geothermal Research, 62, 95–135.

Cox, S.F., 2016, Injection-driven swarm seismicity and permeability enhancement: implications for the dynamics of hydrothermal ore systems in high fluid-flux overpressured faulting regimes-an invited paper. Economic Geology, 111, 559–587.

Dreger, D.S., 2003, TDMT_INV: Time Domain seismic Moment Tensor INVersion. In: Lee, W.H.K., Kanamori, H., Jennings, P.C., and Kisslinger, C. (eds.), International Handbook of Earthquake and Engineering Seismology. Academic Press, London, 81, p. 1627. https://doi.org/10.1016/S0074-6142(03)80290-5

Dziak, R.P. and Fox, C.G., 1999, The January 1998 earthquake swarm at Axial Volcano, Juan de Fuca Ridge: hydroacoustic evidence of seafloor volcanic activity. Geophysical Research Letters, 26, 3429–3432.

Farrell, J., Smith, R.B., Taira, T., Chang, W.-L., and Puskas, C.M., 2010, Dynamics and rapid migration of the energetic 2008–2009 Yellowstone Lake earthquake swarm. Geophysical Research Letters, 37, L19305. https://doi.org/10.1029/2010GL044605

Geshi, N., Shimano, T., Chiba, T., and Nakada, S., 2002, Caldera collapse during the 2000 eruption of Miyakejima Volcano, Japan. Bulletin of Volcanology, 64, 55–68.

Gulia, L., Rinaldi, A.P., Tormann, T., Vannucci, G., Enescu, B., and Wiemer, S., 2018, The effect of a mainshock on the size distribution of the aftershocks. Geophysical Research Letters, 45, 13277–13287.

Han, M., Kim, K.-H., Son, M., and Kang, S.Y., 2017, Current microseismicity and generating faults in the Gyeonju area, southeastern Korea. Tectonophysics, 694, 414–423.

Hatch, R.L., Abercrombie, R.E., Ruhl, C.J., and Smith, K.D., 2020, Evidence of aseismic and fluid-driven process in a small complex seismic swarm near Virginia City, Nevada. Geophysical Research Letters, 47. https://doi.org/10.1029/2019GL085477

Hill, D.P., Langbein, J.O., and Prejean, S., 2003, Relations between seismicity and deformation during unrest in Long Valley Caldera, California, from 1995 through 1999. Journal of Volcanology and Geothermal research, 127, 175–193.

Jung, M.K. and Kyung, J.B., 2013, Source Characteristics of the recent earthquakes for seven years in the southwestern region of the Korean Peninsula. Journal of the Korean Earth Science Society, 34, 59–68. (in Korean with English abstract) https://doi.org/10.5467/

JKESS.2013.34.1.59

Kagan, Y.Y., 1997, Seismic moment-frequency relation for shallow earthquakes: regional comparison. Journal of Geophyscial Research: Solid Earth, 102, 2835–2852.

Kato, A., Fukuda, J., Nakagawa, S., and Obara, K., 2016, Foreshock migration preceding the 2016 Mw 7.0 Kumamoto earthquake, Japan. Geophysical Research Letters, 43, 8945–8953.

Kee, W.S., Kim, S.W., Hong, P.S., Lee, B.C., Cho, D.R., Byun, U.H., Ko, K., Kwon, C.W., Kim, H.C., Jang, Y., Song, K.Y., Koh, H.J., and Lee, H.J., 2020, 1:1,000,000 Geological map of Korea. Korea Institute of Geoscience and Mineral Resources, Daejeon. 1 p.

Kim, S., Rhie, J., and Kimg, G., 2011, Forward waveform modeling procedure for 1-D crustal velocity structure and its application to the southern Korean Peninsula. Geophysical Journal International, 185, 453–468.

Koh, S.-M. and Chang, H.W., 1997, Geological and geochemical characteristics of the Bukok hydrothermal clay deposits in the Haenam area, Korea. Shigen-Chishitsu, 47, 29–40. https://doi.org/10.11456/shigenchishitsu1992.47.29

Korea Meteorological Administration, 2020, Jeonnam Haenam region earthquake occurrence status and additional installation plan for seismic network. (in Korean) http://www.kma.go.kr/notify/press/kma_list.jsp?bid=press&mode=view&num=1193871&page=1&field=subject&text=%C1%F6%C1%F8 [Accessed on 3 October 2020].

Lohman, R.B. and McGuire, J.J., 2007, Earthquake swarms driven by aseismic creep in the Salton Trough, California. Journal of Geophysical Research, 112, B04405.

Minson, S. and Dreger, D.S., 2008, Stable inversion for complete moment tensors. Geophysical Journal International, 174, 585–592.

Mogi, K., 1963, Some discussions on aftershocks, foreshocks and earthquake swarms: the fracture of a semi-infinite body caused by an inner stress origin and its relation the earthquake phenomena. Bulletin of the Earthquake Research Institute, University of Tokyo, 41, 615–658. https://ci.nii.ac.jp/naid/120000866534/

National Emergency Management Agency, 2012, Active Fault Map and Seismic Hazard Map. Report NEMA-Natrue-2009-24, Seoul, 899 p.

Parotidis, M., Shapiro, S.A., and Rothert, E., 2005, Evidence for triggering of the Vogtland swarms 2000 by pore pressure diffusion. Journal of Geophysical Research: Solid Earth, 110, B05S10.

Peng, Z. and Zhao, P., 2009, Migration of early aftershocks following the 2004 Parkfield earthquake. Nature Geoscience, 2, 877–881.

Ross, Z.E., Cochra, E.S., Trugman, D.T., and Smith, J.D., 2020, 3D fault architecture controls the dynamism of earthquake swarms. Science, 368, 1357–1361.

Ross, Z.E., Rollins, C., Cochran, E.S., Hauksson, E., Avouac, J.-P., and Ben-Zion, Y., 2017, Aftershocks driven by afterslip and fluid pressure sweeping through a fault-fracture mesh. Geophysical Research Letters, 44, 8260–8267.

Ruhl, C.J., Abercrombie, R.E., and Smith, K.D., 2017, Spatiotemporal variation of stress drop during the 2008 Mogul, Nevada, earthquake swarm. Journal of Geophysical Research: Solid Earth, 122, 8163–8180.

Ruhl, C.J., Abercrombie, R.E., Smith, K.D., and Zaliapin, I., 2016, Complex spatiotemporal evolution of the 2008 Mw 4.9 Mogul earthquake swarm (Reno Nevada): interplay of fluid and faulting. Journal of Geophysical Research: Solid Earth, 121, 8196–8216.

Ryoo, C.-R., Park, S.-W., and Lee, H., 2014, Geological structures and mineralization in the Yeongnam mineralized zone, Korea. Journal of the Petrological Society of Korea, 23, 1–15.

Scholz, C.H., 2002, The Mechanics of Earthquakes and Faulting (2nd edition). Cambridge University Press, New York, 471 p.

Schorlemmer, D., Wiemer, S., and Wyss, M., 2005, Variations in earthquake-size distribution across different stress regimes. Nature, 437, 539-542.

Shapiro, S.A., Huenges, E., and Borm, G., 1997, Estimating the crust permeability from fluid-injection-induced seismic emission at the KTB site. Geophysical Journal International, 131, F15–18.

Sheen, D.-H. and Shin, J.S., 2010, Earthquake detection thresholds of broadband seismic networks in South Korea considering background seismic noise levels. Journal of the Geological Society of Korea, 46, 31–38 (in Korean with English abstract).

Shelly, D.R., Peng, Z., Hill, D.P., and Aiken, C., 2011, Triggered creep as a possible mechanism for delayed dynamic triggering of tremor and earthquakes. Nature Geoscience, 4, 384–388.

Shelly, D.R., Taira, T., Prejean, S.G., Hill, D.P., and Dreger, D.S., 2015, Fluid-faulting interactions: fracture-mesh and fault-valve behavior in the February 2014 Mammoth Mountain, California, earthquake swarm. Geophysical Research Letter, 42, 5803–5812.

Shin, J.S., Chi, H.C., and Cho, C.-S., 2005, Review on M_L scales in southern Korea. Journal of Korean Geophysical Society, 8, 207–209. (in Korean with English abstract)

Shin, J.S., Seong, Y.-J., and Son, M., 2019, Characterizing the performance of new seismic stations in southeastern region, Korea using seismic noise levels. Journal of the Earthquake Engineering Society of Korea, 23, 321–327. (in Korean with English abstract)

Sibson, R.H., 2020, Dual-driven fault failure in the lower seismogenic zone. Bulletin of the Seismological Society of America, 110, 850–862.

Soh, I., Chang, C., Lee, J., Hong, T.-K., and Park, E-S., 2018, Tectonic stress orientations and magnitudes, and friction of faults, deduced from earthquake focal mechanism inversions over the Korean Peninsula. Geophysical Journal International, 213, 1360–1373.

Son, M., 2016, Relocation of clustered seismic events on the Korean Peninsular using double-difference technique and cross-correlation. Ph.D. Thesis, Seoul National University, Seoul, 125 p.

Son, M., Cho, C.S., Shin, J.S., Rhee, H.M., and Sheen, D.H., 2018, Spatiotemporal distribution of events during the first three months of the 2016 Gyeongju, Korea, earthquake sequence. Bulletin of the Seismological Society of America, 108, 210–217.

Son, M., Shin, J.S., Kim, G., and Cho, C.S., 2015, Epicenter relocation of two 2013 earthquake sequences in the Yellow Sea, Korea, using travel-time double-differences and Lg-wave cross-correlation. Geosciences Journal, 19, 295–303.

Talwani, P. and Acree, S., 1984, Pore pressure diffusion and the mechanism of reservoir-induced seismicity. Pure and Applied Geophysics, 122, 947–965.

Trugman, D.T. and Shearer, P.M., 2017, GrowClust: a hierarchical clustering algorithm for relative earthquake relocation, with application to the Spanish Springs and Sheldon, Nevada, Earthquake sequence. Seismological Research Letters, 88, 379–391.

Wessel, P., Smith, W.H.F., Scharroo, R., Luis, J., and Wobbe, F., 2013, Generic mapping tools: improved version released. Eos, Transactions American Geophysical Union, 94, 409–410.

Woo, J.-U., Rhie, J., Kim, S., Kang, T.-S., Kim, K.-H., and Kim, Y., 2019, The 2016 Gyeongju earthquake sequence revisited: aftershock interactions within a complex fault system. Geophysical Journal International, 217, 58–74.

Yang, S.-J., Duuring, P., and Kim, Y.-S., 2013, Structural genesis of the Eunsan and Moisan low-sulphidation epithermal Au-Ag deposits, Seongsan district, Southwest Korea. Mineralium Deposita, 48, 467–483.

https://doi.org/10.1007/s12303-020-0043-6